Diurnal changes in middle atmospheric H2O and O3: Observations in the Alpine region and climate models

Alexander Haefele, K. Hocke, N. Kämpfer, Philippe Keckhut, Marion Marchand, Slimane Bekki, Béatrice Morel, T. Egorova, E. Rozanov

Diurnal changes in middle atmospheric H_2O and O_3: Observations in the Alpine region and climate models

A. Haefele,[1] K. Hocke,[1] N. Kämpfer,[1] P. Keckhut,[2] M. Marchand,[3] S. Bekki,[3] B. Morel,[4] T. Egorova,[5] and E. Rozanov[5,6]

Received 31 January 2008; revised 26 June 2008; accepted 2 July 2008; published 5 September 2008.

[1] In this paper we investigate daily variations in middle atmospheric water vapor and ozone based on data from two ground-based microwave radiometers located in the Alpine region of Europe. Temperature data are obtained from a lidar located near the two stations and from the SABER experiment on the TIMED satellite. This unique set of observations is complemented by three different three-dimensional (3-D) chemistry-climate models (Monitoring of Stratospheric Depletion of the Ozone Layer (MSDOL), Laboratoire de Météorologie Dynamique Reactive Processes Ruling the Ozone Budget in the Stratosphere (LMDz-REPROBUS), and Solar Climate Ozone Links (SOCOL)) and the 2-D atmospheric global-scale wave model (GSWM). The first part of the paper is focused on the first Climate and Weather of the Sun-Earth System (CAWSES) tidal campaign that consisted of a period of intensive measurements during September 2005. Variations in stratospheric water vapor are found to be in the order of 1% depending on altitude. Meridional advection of tidal nature is likely to be the dominant driving factor throughout the whole stratosphere, while vertical advection becomes more important in the mesosphere. Observed ozone variations in the upper stratosphere and lower mesosphere show amplitudes of several percent in accordance with photochemical models. Variations in lower stratospheric ozone are not solely governed by photochemistry but also by dynamics, with the temperature dependence of the photochemistry becoming more important. The second part presents an investigation of the seasonal dependence of daily variations. Models tend to underestimate the H_2O diurnal amplitudes, especially during summer in the upper stratosphere. Good agreement between models and observations is found for ozone in the upper stratosphere, which reflects the fact that the O_3 daily variations are driven by the photochemistry that is well modeled.

Citation: Haefele, A., K. Hocke, N. Kämpfer, P. Keckhut, M. Marchand, S. Bekki, B. Morel, T. Egorova, and E. Rozanov (2008), Diurnal changes in middle atmospheric H_2O and O_3: Observations in the Alpine region and climate models, *J. Geophys. Res.*, *113*, D17303, doi:10.1029/2008JD009892.

1. Introduction

[2] One important driver of daily variations in middle atmospheric trace constituents is photodissociation. Depending on altitude and constituent these changes can show large amplitudes and abrupt transitions at sunrise or sunset quite similar to step functions as in the case of ozone in the upper stratosphere and mesosphere. In addition the periodic heating of the atmosphere by absorption of solar radiation by stratospheric ozone and tropospheric water vapor as well as by latent heat release excites planetary-scale waves that propagate in the whole atmosphere. The sun-synchronous waves of wavenumbers 1 and 2 are denoted as the diurnal and semidiurnal migrating tides. These tides are spatiotemporal disturbances in temperature, density, pressure and wind which in turn produce variations in the distribution of constituents through modulation of temperature-dependent reaction rates, compression, and advection given a nonvanishing gradient in concentration.

[3] The diurnal variation of upper stratospheric and mesospheric ozone has been intensively discussed [*Prather*, 1981; *Pallister and Tuck*, 1983; *Vaughan*, 1984]. Odd oxygen ($O_x = O + O_3$) is produced during the day through photolysis of molecular oxygen. In the middle stratosphere (up to 40–44 km) all odd oxygen is in the form of ozone. As a consequence, ozone volume mixing ratios are enhanced during the day and reach a maximum in the late afternoon. At higher levels the $[O]/[O_3]$ ratio increases owing to its inverse dependence on density. Therefore more and more of

[1]Institute of Applied Physics, University of Bern, Bern, Switzerland.
[2]Service d'Aéronomie du CNRS, University of Versailles, Verrières-le Buisson, France.
[3]Service d'Aéronomie, University Pierre et Marie Curie, Paris, France.
[4]Université de la Réunion, La Réunion, France.
[5]Physical-Meteorological Observatory, World Radiation Center, Davos, Switzerland.
[6]Institute for Atmospheric and Climate Science, ETH Zurich, Zurich, Switzerland.

0148-0227/08/2008JD009892

the odd oxygen resides as atomic oxygen and ozone shows a strong depletion during the day. After dusk all the O recombines with O_2 to O_3. In addition, odd oxygen is catalytically destroyed during the day by NO_x, ClO_x and HO_x. These processes lead to a characteristic daytime variation in ozone and to a dependence of the night/day ratio of ozone on water vapor, which is the main source of HO_x compounds [*Vaughan*, 1984; *Marsh et al.*, 2003].

[4] The temperature dependence of the ozone concentration near the stratopause was first noted by *Barnett and Pyle* [1975]. *Rood and Douglass* [1985] and *Douglass et al.* [1985] investigated the relationship between ozone and temperature perturbations taking photochemistry and dynamics into account and found that a wide range of phase relationships can be observed depending on the importance of the dynamical terms. *Froidevaux et al.* [1989] analyzed the coupling of ozone and temperature taking into account only photochemistry. In that case the phase relationship is governed by the ratio of the ozone chemical relaxation time, t_c, to the period of the temperature perturbation, t_p. For $t_p/t_c \gg 1$ photochemical equilibrium is always maintained and the perturbation in ozone mixing ratio, f'_{O_3}, can be estimated from the temperature perturbation, T', as

$$f'_{O_3} = -\frac{\Theta_E f_{O_3}}{T^2} T', \tag{1}$$

where f_{O_3} is the ozone mixing ratio, T is temperature, Θ_E is the equilibrium sensitivity coefficient and its value is in the range of 1400 K [*Barnett and Pyle*, 1975] depending on altitude and for pure oxygen photochemistry. In case of photochemical equilibrium, ozone and temperature are out of phase by 12 h. For temperature perturbations on a timescale of less than about $4t_c$, equilibrium cannot be maintained and as a consequence the sensitivity decreases and ozone leads temperature by 6 h [*Froidevaux et al.*, 1989]. In case of very fast temperature perturbations, $t_p/t_c < 0.1$, ozone no longer shows any response. Some initial results on the nature of short-term (1–3 h) fluctuations of the ozone volume mixing ratio around the stratopause have been reported by *Hocke et al.* [2006].

[5] Adiabatic vertical transport also constitutes an important link between temperature and ozone revealing a positive correlation for positive vertical gradients (ozone increases with height) and negative correlation for negative vertical gradients. The quantitative connection between temperature perturbation and vertical displacement is given in section 2.3.

[6] In contrast to ozone little is known about the diurnal behavior of middle atmospheric water vapor because the variations are small and difficult to measure [*Randel*, 1990]. H_2O enters the middle atmosphere through the tropical tropopause or is formed by methane oxidation in the stratosphere [see *Randel et al.*, 1998, and references therein]. The long chemical lifetime of water vapor makes it a good tracer for atmospheric transport processes. Daily variations of H_2O in the middle atmosphere are therefore expected to be dominated by advection. Large vertical gradients are found in the lower mesosphere and meridional gradients are maximal during autumn in the stratosphere. However, diurnal amplitudes in vertical and meridional winds are small at these altitudes and hence amplitudes in water vapor are expected in the order of 1% or less, only. To our knowledge this effect has so far not been observed successfully. The small amplitudes require a large amount of observations at a fixed location in order to reduce statistical noise. These requirements are met by the ground based radiometers reported here.

[7] In order to improve our knowledge of the composition change under the combined effect of photochemistry and tidal advection processes, observations are required. Up to now there exists a variety of numerical models dedicated to climate investigations, data assimilation, ozone-climate processes, planetary waves or other issues. Many of such models have been investigated with respect to diurnal variations [see, e.g., *McLandress*, 1997; *Hecht et al.*, 1998; *Morel et al.*, 2004]. Since the daily variations result from dynamical-radiative interaction processes, their investigation and validation with observations provide helpful information for the evolution and improvement of the numerical models.

[8] In this work we investigate daily variations in middle atmospheric water vapor, ozone and temperature observed at Alpine NDACC stations (Network for the Detection of Atmospheric Composition Change). The observed daily variations are compared to the 3-D climate models MSDOL [*Bertaux et al.*, 1999], LMDz [*Eyring et al.*, 2006] (both are expected to implicitly include tides), SOCOL [*Egorova et al.*, 2005] and to the 2-D linearized global scale wave model GSWM [*Hagan et al.*, 1999], specifically developed to reproduce tides of the dynamical parameters. The use of both observational and model data should increase the confidence in the derived diurnal cycles and allow for a better characterization.

[9] The paper is organized as follows. In section 2 the data sets obtained from measurements and models are presented, and the derivation of daily variations is described. Section 3 is dedicated to the first CAWSES campaign with a detailed description and qualitative comparison of the daily variations derived from observational and model data. In section 4 the analysis is extended to a longer time period, and seasonal variations in the daily cycles are investigated with special focus on lower mesospheric water vapor. A summary and conclusions are given in section 5.

2. Data Sets and Analysis

2.1. Observations

2.1.1. MIAWARA

[10] The composition of the middle atmosphere is investigated with two ground based microwave radiometers operated in Switzerland. The Middle Atmospheric Water Vapor Radiometer, MIAWARA [*Deuber et al.*, 2004], is run by the University of Bern. The measurement site is close to Bern (47°N,7°E) and is one of the Alpine NDACC stations (Network for the Detection of Atmospheric Composition Change). MIAWARA measures the pressure broadened emission line of H_2O at 22 GHz which allows to retrieve vertical water vapor profiles between 25 and 65 km at a sampling rate of one profile per hour. The back end consists of an acousto-optical spectrometer with a frequency resolution of 1.2 MHz and for the inversion a bandwidth of 300 MHz centered around the line center frequency has been chosen. The ARTS [*Buehler et al.*,

2005] and QPack [*Eriksson et al.*, 2005] software packages are used for the retrieval. The width of the averaging kernels lies between 12 and 18 km at altitudes of 30 and 50 km, respectively. The measurement is equally accurate for daytime and nighttime. Rain, however, does not allow to take measurements. The total error (sum of systematic error, noise and retrieval smoothing) is less than 30% between 35 and 55 km and less than 40% between 30 and 65 km. Precision, however, is more important in the derivation of daily variations and is estimated from the standard deviation of the retrieved water vapor values and is less than 6% over the whole altitude range. In order to detect variations in H_2O of less than 1% a time period of at least one month is required.

[11] Within the investigation of such small variations also instrumental effects and calibration issues have to be considered. The spectra measured at the ground have to be corrected for the troposphere before information from the middle atmosphere can be retrieved. This correction is a pure scaling of the spectrum and it depends mainly on the tropospheric opacity. Any time-dependent error in this scaling factor could produce diurnal variations in the retrieved water vapor values. We thus compared carefully the diurnal cycles in opacity with those in water vapor and could not find any correlation that is persistent throughout the whole year. Also the seasonal evolution of the diurnal amplitude in opacity differs significantly from the one in water vapor. The same analysis has been done with receiver temperature and water vapor revealing the same results. There is no evidence that the diurnal variations in water vapor reported in this paper are driven by the tropospheric correction or by a diurnally evolving error in the calibration.

2.1.2. SOMORA

[12] The Stratospheric Ozone Monitoring Radiometer, SOMORA, is run by MeteoSwiss at Payerne (47°N,7°E), another Alpine NDACC station [*Hocke et al.*, 2007]. It measures the pressure broadened emission line of O_3 at 142 GHz allowing to retrieve vertical profiles of volume mixing ratio between 25 and 55 km with a vertical resolution of 8–10 km and a time resolution of 30 min by using the optimal estimation method of *Rodgers* [1976]. The back end contains two acousto-optical spectrometers and the total of 3072 channels is reduced to 57 channels with a channel width of 0.3–100 MHz. The total error (sum of systematic error, noise, and retrieval smoothing error) is less than 15% at altitudes from 20 to 40 km and around 30% in the lower mesosphere [*Calisesi*, 2003]. The precision is derived from the standard deviation of the nighttime ozone values between 20 and 4 h local solar time and lies between 2 and 3% of the mean nighttime value below 40 km and increases to 7% at 55 km. The instrument is in operation since the year 2000. Both radiometers are run continuously within NDACC.

2.1.3. Retrieval Issues

[13] In the retrieval process information from the measurement, for example, the intensity spectrum of a transition line of the molecule of interest, is added to a first guess of the vertical distribution of the constituent under consideration, namely to the a priori profile. The retrieved profile is thus a mix of an a priori guess and information from the measurement and it is characterized by the averaging kernel, AVK, which is the response of the retrieved profile to a change in the true atmosphere. The FWHM and the area of the AVK functions are measures of the vertical resolution and the sensitivity of the retrieval to the measurement. To compare the retrieved profile to an other measured or modeled profile with higher vertical resolution, the AVK should be taken into account. However, we decided not to take the AVK into account in the analysis for the following reasons: In case of water vapor only little is known about daily variations in the middle atmosphere. As it is the aim to characterize these variations it does not make sense to impose the deficiencies of the observations to the model data even though this would improve the comparison. Interesting features would get lost in the model data that are likely to happen in the real atmosphere as well but that do not show up in the observations owing to their limitations in resolution and sensitivity. As a control most of the analysis has been done also under consideration of the AVK and whenever large discrepancies between observations and models can be attributed to AVK effects it is discussed in the text.

[14] The altitude range where the contribution of the measurement is high is mainly given by the spectral bandwidth and the resolution of the measurement. The thermal noise on the measured intensity spectrum is mapped to the ozone and water vapor profiles by the retrieval. Hence the retrieved mixing ratio values are most noisy at altitudes where the contribution of the measurement is largest and decrease toward the upper and lower boundary with increasing contribution of the a priori profile. This explains why the time series of water vapor as shown in Figure 3 in section 3.1.1 are more noisy at 3.14 hPa than at 0.10 hPa, for instance. The decreasing contribution of the measurement to the retrieved profile leads to an underestimation of the daily variations at the upper and lower limit of the altitude range as the daily variations are not accounted for in the a priori profile. The investigated altitude range is restricted to the levels where the contribution of the a priori value is less than 40%. A priori information on H_2O is based on the US standard atmosphere and is kept constant for all seasons. The a priori profiles of O_3 are two climatological mean profiles for summer and winter. Pressure and temperature profiles are also required to retrieve the volume mixing ratio profiles and ECMWF analyses at a 6-hourly basis are used.

2.1.4. OHP Lidar

[15] Since 1979 routine lidar measurements are conducted at the Observatory of Haute-Provence (OHP) in France (42°N,7°E), another Alpine NDACC station. This site is located 3° south from Bern and 360 km apart which is quite small compared to tidal scales. During clear nights, the lidar can be operated continuously and provides hourly temperature profiles between 30 and 80 km. The statistical noise is better than 1 K below 70 km and improves at lower altitudes up to a few tenth of degree at 30 km [*Hauchecorne and Chanin*, 1980]. Because this lidar uses the 532 nm wavelength, it cannot operate during daytime with the same accuracy and only part of the diurnal cycle can be retrieved. However, the diurnal evolution can be observed during nighttime and the tidal signature can be extracted from a composite time series (see section 2.3).

2.2. Models

2.2.1. MSDOL

[16] The Monitoring of Stratospheric Depletion of the Ozone Layer system, MSDOL [*Bertaux et al.*, 1999], is a

3-D dynamics-chemistry-transport mechanistic model running with an interactive ozone chemistry using the REPROBUS (Reactive Processes Ruling the Ozone Budget in the Stratosphere) code [*Lefèvre et al.*, 1994, 1998]. The ozone field can be fully interactive or adjusted by data assimilation [*Bertaux et al.*, 1999]. The model covers the altitude range from 10 to 80 km with a resolution of about 3 km in the vertical, 5° in latitude and 11.6° in longitude. For this study MSDOL has been running in an interactive mode without data assimilation. However, to produce realistic values horizontal wind, temperature and geopotential fields below 10 hPa have been nudged to European Center for Medium range Weather Forcast (ECMWF) daily reanalysis data that are available every 6 h. The ability of MSDOL to reproduce tides has been investigated by *Morel et al.* [2004]. Radiative forcing is included in the dynamical equations based on solar heating due to O_3 and O_2 absorption, and CO_2 infrared cooling. The solar heating due to the absorption of UV radiation by O_3 and O_2 is computed using the parameterization of *Strobel* [1978], with coefficients updated from *Zhu* [1994]. CO_2 cooling rates for the 15 and 4.3 μm bands are calculated using the algorithm supplied by *Fels and Schwarzkopf* [1981] and *Schwarzkopf and Fels* [1985]. Gravity wave drag is simulated using a simple Rayleigh friction. The chemical model includes 33 chemical species and 5 chemical families. The species are grouped into two categories: short-lived species are assumed to be in photochemical equilibrium in their family; long-lived species are affected by both photochemistry and transport. The advection scheme implemented in MSDOL is a van Leer Eulerian scheme [*van Leer*, 1977].

2.2.2. LMDz

[17] LMDz-REPRO (LMD: Laboratoire de Météorologie Dynamique, REPRO: see section 2.2.1) is a fully coupled 3-D Chemistry-Climate Model (CCM) [*Eyring et al.*, 2006] that is one of the components of the IPSL (Institut Pierre-Simon Laplace) earth system model. The dynamical model used is the stratospheric extension of the LMDz fourth-generation atmospheric GCM described by *Lott et al.* [2005]. It is a gridpoint model. In the horizontal direction, the equations are discretized on a staggered latitude-longitude Arakawa-C grid. It currently uses a uniform resolution of 2.5° in latitude and 3.75° in longitude. The vertical coordinate is a hybrid sigma pressure. It currently uses 50 levels with the upper boundary near 65 km. The resolution in the stratosphere varies slowly from 1 km at 12 km to 3 km at 50 km and reaches 6 km at the model top. The salient features of the physical parameterizations used in the model are a radiation scheme based on the ECMWF scheme [*Morcrette*, 1989], a convection scheme based on work by *Tiedke* [1989], a Subgrid Scale Orography (SSO, which forces orographic gravity waves) scheme based on work by *Lott and Miller* [1997] and *Lott* [1999], and a Doppler-spread nonorographic gravity waves scheme based on work by *Hines* [1997] and adapted from *Manzini and McFarlane* [1998]. The transport of tracers is calculated using the Van Leer scheme I (a first-order volume finite scheme with slope limitation) [*van Leer*, 1977; *Hourdin and Armengaud*, 1999]. The model is interactively coupled to the module of atmospheric chemistry from the REPROBUS chemistry transport model. The module contains a comprehensive stratospheric chemistry scheme. It describes a large range of chemical reactions associated with species from O_x, HO_x, ClO_x, BrO_x and NO_x families and source gases. The model includes both gas-phase chemistry and heterogeneous chemistry on aerosols and polar stratospheric clouds. The model-calculated fields of radiatively active species such as ozone or CH_4 are used as input variables of the radiative routine. As a result, chemistry impacts dynamics. In return, the model-calculated winds are used to transport the chemical tracers and the model-calculated temperatures are used in the chemical module. Therefore, dynamics impacts chemistry. Because of this configuration, most CCMs are fully interactive and are probably the most suitable tools to make predictions of the atmospheric composition in a changing climate.

2.2.3. SOCOL

[18] The chemistry-climate model SOCOL (Solar Climate Ozone Links) is a combination of the middle atmosphere MA-ECHAM4 General Circulation Model and a modified version of the atmospheric chemistry-transport model MEZON (Model for the Evaluation of Ozone Trends). The MA-ECHAM4 model is the middle atmosphere version of ECHAM4 (European Center/Hamburg 4), which has been developed at the Max Planck Institute for Meteorology in Hamburg, Germany. It is a spectral model with T30 horizontal truncation resulting in a grid spacing of about 3.75°; in the vertical direction the model has 39 levels in a hybrid sigma-pressure coordinate system spanning the model atmosphere from the surface to 0.01 hPa; a semi-implicit time stepping scheme with weak filter is used with a time step of 15 min for dynamical processes and physical process parameterizations; full radiative transfer calculations are performed every 2 h, but heating and cooling rates are calculated every 15 min. The model includes the parameterizations for the orographic gravity wave and momentum flux deposition due to a continuous spectrum of vertically propagating gravity waves. A more detailed description of MA-ECHAM4 is given by *Manzini and McFarlane* [1998, and references therein]. The chemical-transport part of the model [*Rozanov et al.*, 1999; *Egorova et al.*, 2003] simulates 41 chemical species from the oxygen, hydrogen, nitrogen, carbon, chlorine and bromine groups, which are determined by 202 gas-phase and photolysis reactions. The model also takes into account 16 heterogeneous reactions. The chemical solver is based on the pure implicit iterative Newton-Raphson scheme. The reaction coefficients are taken from *Sander et al.* [2000]. The photolysis rates are calculated at every 2-hour-long chemical-transport step using a look-up-table approach. This parameterization takes into account the photodissociation in the spectral region between 120 and 170 nm, which is significant for the chemistry of the mesosphere. The transport of all considered species is calculated using the hybrid numerical advection scheme proposed by *Zubov et al.* [1999]. MA-ECHAM4 and MEZON are interactively coupled by the radiative forcing induced by ozone, water vapor, methane, nitrous oxide, and chlorofluorocarbons. The CCM SOCOL has been comprehensively evaluated by *Egorova et al.* [2005] and *Rozanov et al.* [2005] as well as in the framework of the SPARC CCMval campaign [*Eyring et al.*, 2006] and reviled some problems. Here in this study we use

version 2.0 of CCM SOCOL in which found problems have been corrected and described in detail by *Schraner et al.* [2008].

2.2.4. GSWM

[19] The GSWM is a 2-D, linearized, steady state numerical tidal and planetary wave model which extends from the ground to the thermosphere. Background temperatures and densities are specified by MSISE90 [*Hedin*, 1991]. Below 20 km the background winds are taken from the semiempirical model of *Groves* [1995, 1997], but the stratomesospheric jets and mesopause region winds are based upon Upper Atmosphere Research Satellite (UARS) High Resolution Doppler Interferometer (HRDI) climatologies [*Hagan et al.*, 1999]. Above 125 km mean zonal winds are from HWM93 [*Hedin*, 1991, 1996]. GSWM employs the tropospheric tidal heating formulae of *Groves* [1982] which are based on 3-month averaged global models of specific humidity centered on January, April, July, and October. These heating rates were linearly interpolated for the GSWM-00 calculations. In the stratosphere, throughout the mesosphere, and into the lower thermosphere GSWM tidal heating is based upon a parameterization reported by *Strobel* [1978].

[20] For this study we used GSWM-00 which produces monthly migrating tidal climatologies and which is a extension to GSWM-98 [*Hagan et al.*, 1999]. MSDOL and GSWM have been compared in the work of *Morel et al.* [2004] with respect to tides. The diurnal amplitude in temperature shows a maximum at midlatitudes at around 45 km, corresponding to the region of maximum heating by ozone. This maximum is described well by both models but is generally smaller in GSWM. Above 60 km however, the diurnal amplitudes predicted by GSWM are larger than in MSDOL by a factor of 1.5.

2.3. Derivation of Daily Variations

[21] A statistical approach has to be chosen to derive daily variations from climate model and radiometer data: Each obtained value of volume mixing ratio, f, is transformed to the relative deviation from the daily mean: $f^* = (f - \overline{f})/\overline{f}$, where $\overline{f}$ is the daily mean. These deviations are binned into i intervals of $24/i$ h based on local solar time ($i = 24$ for ozone and $i = 12$ for water vapor). The mean values of each of these intervals give finally the mean deviation from the daily mean, the daily variation. The errors of these mean values are estimated by $\sigma_i/\sqrt{n_i}$ where σ_i is the standard deviation, and n_i is the number of data points within the interval i. As noise on the retrieved values by far exceeds the amplitudes of daily variations, the analysis requires at least one month of data. This makes it impossible to study day to day variations but still allows to study the seasonal behavior of the daily cycle. Additionally, sine and cosine waves with periods of 12 and 24 hour periods are fitted to the daily cycles and the amplitude and phase of the diurnal and semidiurnal component are derived from the coefficients. The phase is defined as the local solar time of the maximum. Even though harmonic decomposition may not always be a good representation of the physics behind the daily variations of atmospheric composition and step or tent functions might be more appropriate it is still useful for direct comparison purposes.

[22] In case of lidar a lot of resources are required for the operation. Full night measurements are only performed on a campaign basis. In addition to the partial coverage of the diurnal cycle, tides are also masked by the propagation of gravity waves. Several nights are usually averaged to get a better signal to noise ratio. However the mean diurnal cycle due to tides can also interact with longer periods and the analysis is not trivial [*Morel et al.*, 2002]. With some assumption about the phase, or during winter time when longer dark periods allow to cover 14 h of continuous measurements, tidal amplitudes of temperature can be retrieved by fitting a 12- and a 24-hour cosine wave to the time series [*Gille et al.*, 1991; *Keckhut et al.*, 1996].

[23] In case of GSWM the daily constituent variations are calculated analytically as follows from GSWM winds and monthly mean meridional gradients derived from MLS/Aura satellite data [*Froidevaux et al.*, 2006] and monthly mean vertical gradients derived from radiometer data. To a first approximation the contributions from zonal, meridional and vertical advection can be calculated separately and added together in order to get the total perturbation. The ith component of the displacement, $d_i(t, z)$, at time t and altitude z is obtained by integration of the according wind component. Multiplication of $d_i(t, z)$ with the gradient in volume mixing ratio along the dimension i, $\nabla_i f$, leads to the constituent perturbation

$$f'(t,z) = -d_i(t,z)\nabla_i f. \tag{2}$$

If adiabatic vertical motion is assumed the vertical displacement, $d_z(t, z)$, can also be estimated from the temperature perturbation as follows [*Ehhalt et al.*, 1983]:

$$d_z = -\frac{T'}{\overline{T}}\frac{g}{N^2}, \tag{3}$$

where T', $\overline{T}$ and N^2 are the temperature perturbation, the mean temperature and the Brunt-Väisälä frequency squared, respectively.

3. Observations During the First CAWSES Campaign

[24] CAWSES (Climate and Weather of the Sun-Earth System) is an international program sponsored by SCOSTEP (Scientific Committee on Solar-Terrestrial Physics) focused on the space environment and its impacts on life and society. Within this project coordinated campaigns on tides are organized to study their influence from the troposphere to the thermosphere. The first CAWSES campaign, herein after referred to as C1, took place in September and October 2005.

[25] During C1 both radiometers were running continuously collecting 600 water vapor and 1800 ozone profiles. The lidar was in operation whenever the conditions allowed it covering the times specified in Figure 1. As discussed in section 2.2 the MSDOL model has been nudged to ECMWF reanalysis data to produce realistic atmospheric conditions while LMDz was run in fully interactive mode for the year

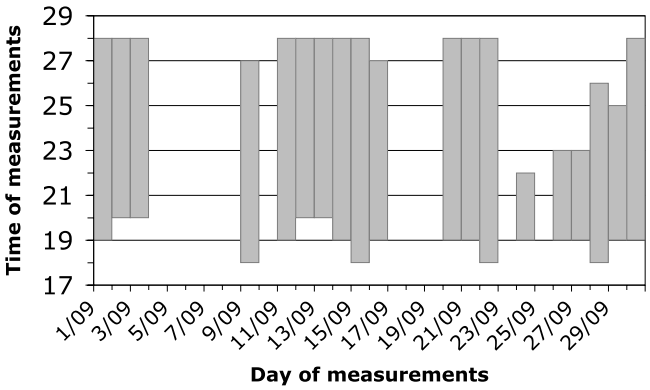

Figure 1. Time coverage of lidar measurements at OHP from 1700 local time (LT) to 0500 LT during the first CAWSES campaign in September/October 2005.

2005. The SOCOL run does not cover the year 2005 and is not taken into account in this Section.

3.1. Time Series

[26] The vertical distribution of water vapor and ozone are characterized by a pronounced maximum at 45–55 km and 30–35 km, respectively, as shown in Figure 2. These maxima are herein after called peak heights. Large variability is found among the different data sets in case of both ozone and water vapor. The peak heights range from ~50 km (MIAWARA) to ~60 km (SOCOL) in case of water vapor with maximum values between 5 ppmv (LMDz) and 6.5 ppmv (SOCOL). The peak heights in ozone are found between 30 km (MSDOL) and 36 km (SOMORA) and the maximum values are between 7 ppmv (SOCOL) and 8.25 ppmv (MSDOL).

3.1.1. Water Vapor

[27] Water vapor has been analyzed at 3.14 hPa (upper stratosphere, below peak height) and at 0.10 hPa (lower mesosphere, above peak height) and results are shown in the top two panels of Figure 3. At 3.14 hPa a diurnal cycle is apparent in the observations with a double bumped maximum of 1% of the daily mean between 6 and 12 h and a clear minimum at 18 h. The MSDOL and LMDz models are in good agreement with the observations showing enhanced water vapor values between midnight and noon followed by a minimum short after 18 h. The observed diurnal evolution at 0.10 hPa is similar to the one observed at the lower level with a pronounced maximum at 4 h but an amplitude less than 0.5%. MSDOL shows a strong semidiurnal component at this level. It has to be noted that the measurement does not have the full sensitivity at this level and the amplitude is

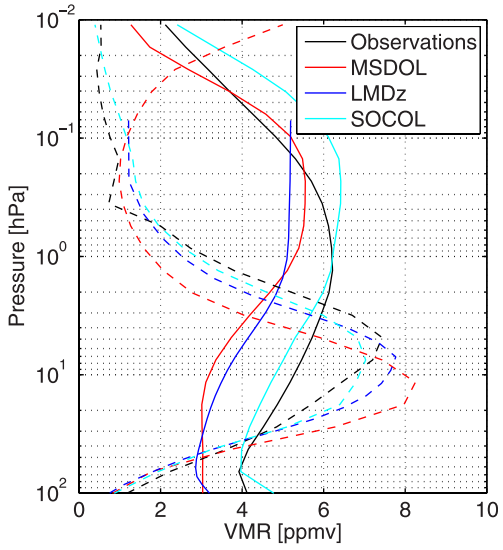

Figure 2. Mean water vapor (solid line) and ozone (dashed line) profiles of the first CAWSES campaign in September/October 2005. MIAWARA-radiometer (black), SOMORA-radiometer (black), MSDOL (red), LMDz (blue), and SOCOL (cyan).

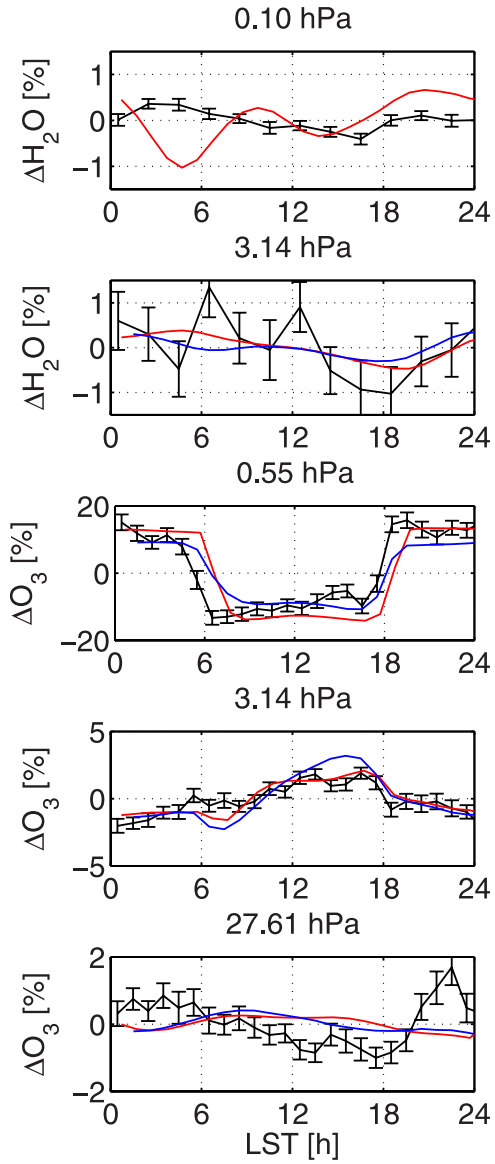

Figure 3. Mean relative daily variations of H_2O and O_3 volume mixing ratios at fixed pressure levels as a function of local solar time and averaged for the first CAWSES campaign in September/October 2005 derived from observations (black line) and from models: MSDOL (red line) and LMDz (blue line). The error bars represent the errors of the mean values as described in section 2.3.

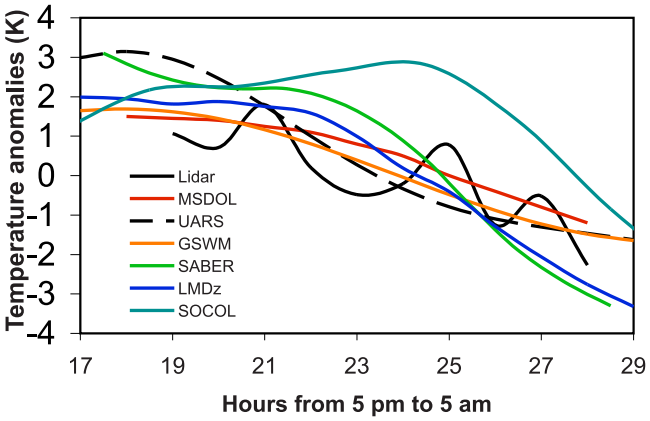

Figure 4. Nighttime evolution of the temperature anomaly with respect to the nighttime mean between 1700 LT and 0500 LT at 45 km. UARS refers to the statistical model described by *Keckhut et al.* [1996].

likely to be underestimated. The LMDz model is close to its top and is not shown at this level.

3.1.2. Ozone

[28] Ozone cycles are derived for the levels at 27.61 hPa (lower stratosphere, below peak height), 3.14 hPa (stratosphere, above peak height) and 0.55 hPa (stratopause, above peak height). Observations show a pronounced diurnal cycle at 27.61 hPa with a maximum of 1% short before midnight. Both MSDOL and LMDz are out of phase with the observations by 6 h and show smaller amplitudes. In the observations a phase change of 12 h takes place between the 27.61 and the 3.14 hPa level. At 3.14 hPa observed ozone shows a maximum around 16 h as a consequence of the production of odd oxygen through photolysis and the low $[O]/[O_3]$ ratio. The peak to peak amplitude is around 5% which is in agreement with photochemical models [*Pallister and Tuck*, 1983; *Ricaud et al.*, 1994]. The SOMORA measurements confirm nicely the predictions of photochemical models about midstratospheric ozone. Observational evidence of this feature has been reported by *Connor et al.* [1994], *Huang et al.* [1997] and very recently by *Huang et al.* [2008] who's results derived from TIMED/SABER are in good agreement with our observations. MSDOL is almost in perfect agreement with the observations at this level. The flat shaped daytime enhancement is an indication of catalytic destruction of ozone. LMDz does not show any indication of daytime depletion at this level and overestimates the amplitude in ozone. At 0.55 hPa ozone is dramatically depleted in the daytime as most O_x resides in the form of atomic oxygen because the $[O]/[O_3]$ ratio increases with decreasing air density. The peak to peak amplitude is around 25% (Figure 3) again in agreement with photochemical models [*Vaughan*, 1984; *Ricaud et al.*, 1994; *Schneider et al.*, 1999]. The night-day differences are well reproduced by MSDOL and LMDz but a time lag of 2 h with respect to the observations is noted.

3.1.3. Temperature

[29] The diurnal evolution of temperature can be observed in the stratosphere by lidar. The comparison with the different models reveal a quite good agreement as shown in Figure 4. It has to be noted that the SOCOL run does not cover the year 2005 and the data shown in Figure 4 is for the year 2000. A statistical tidal model was developed using UARS data [*Keckhut et al.*, 1996] for the OHP latitude and is also in good agreement with OHP observations with an amplitude slightly larger and a small phase shift of a few hours. The recombined time series from monthly mean tidal analysis from SABER data [*Zhang et al.*, 2006] also show larger amplitudes but agree well in terms of phase. No accurate hourly temperature data could be retrieved in the mesosphere from lidar measurements as the variability is too high and no systematic diurnal evolution can be extracted from the noise.

3.2. Vertical Structure

[30] Diurnal anomalies around the altitudes where direct forcing applies (photodissociation or direct radiative heating) are not expected to follow sinusoid functions. However, to investigate the diurnal evolution with altitude the mean daily variations of water vapor and ozone derived from observations have been decomposed into the diurnal and semidiurnal components at all pressure levels. The vertical structure of the amplitude and phase of the diurnal component is shown in Figure 5. The phase is defined as the local solar time of the maximum.

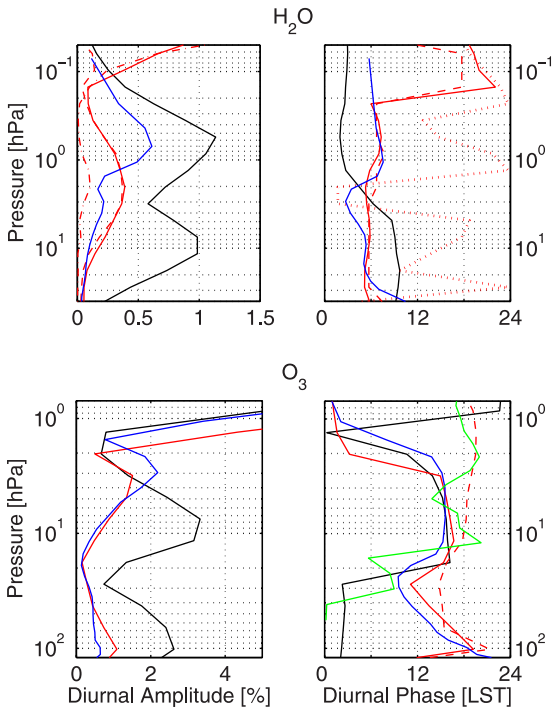

Figure 5. (top) Vertical profiles of the amplitude and phase of the diurnal component of water vapor variations derived from observations (black line), MSDOL (red line), and LMDz (blue line) averaged for the first CAWSES campaign in September/October 2005. The phase is defined as the local solar time of the maximum. The contributions of meridional (red dashed line) and vertical advection (red dash-dotted line), respectively, derived from MSDOL winds and volume mixing ratio gradients according to equation (2) are shown as well. (bottom) Vertical profile of amplitude and phase of the daily variation in ozone from observations (black line), MSDOL (red line), and LMDz (blue line). The temperature phases derived from MSDOL (red dashed line) and SABER data (green line) are also shown.

Table 1. Coverage of the Data Sets

Data Set	Time Period
MIAWARA	Jan 2003 to Sept 2006
SOMORA	Jan 2003 to Dec 2006
SABER	2002–2006
MSDOL	Sept 2004 to March 2006
LMDz	2005
SOCOL	Jan 1998 to Dec 2000

3.2.1. Water Vapor

[31] The observed diurnal amplitude in H_2O shows two distinct maxima at 10 hPa and 0.6 hPa with values around 1%. Above 0.6 hPa the amplitude does not increase as one would expect because of the decreasing contribution of the measurement to the retrieved value (see section 2.1). The phase change from 9 h to 3 h at 3 hPa coincides with the pressure level of a local minimum in amplitude.

[32] The diurnal amplitudes derived from the model data show similar vertical structures with local maxima in the stratosphere but they are smaller than the observed amplitudes. The maxima are found at 0.7 hPa in LMDz and at 2 hPa in MSDOL data, respectively. In addition to the full MSDOL model also the contributions from meridional and vertical advection according to equation (2) are presented in Figure 5. According to MSDOL meridional advection is the main driver of the diurnal variation in stratospheric water vapor. Semidiurnal variations are caused by vertical and meridional advection to the same extent but reach only half of the amplitude of the diurnal component (not shown here). The interaction of vertically decreasing meridional gradients with increasing wind amplitudes above ≈3 hPa leads to a local maximum in the diurnal amplitude at 2 hPa. Above 0.10 hPa vertical advection starts to govern daily variations and the diurnal amplitude shows a fast increase with height because of the amplification of the tidal waves with decreasing density. LMDz does not show this feature because the upper boundary of this model is at ≈0.10 hPa. In the stratosphere simulated amplitudes are generally smaller than observed. The phases as simulated by MSDOL and LMDz are very constant throughout the stratosphere and show only little variation below 0.2 hPa. Compared to the observations, MSDOL is 3 h in advance below 3 hPa and 3-4 h behind above 3 hPa. Above 0.2 hPa MSDOL reveals very different amplitudes and phases suggesting different mechanisms for daily variations.

3.2.2. Ozone

[33] The vertical structure of diurnal amplitude and phase in ozone is presented in the bottom panels of Figure 5. Observations show a local maximum in amplitude of 3% at 10 hPa coincident with the level of the maximum ozone volume mixing ratio (Figure 2). Above 2 hPa amplitudes increase to high values as predicted by photochemistry. Between 20 and 3 hPa the diurnal phase is constant at 14 h and an abrupt change occurs at 2 hPa where the phase changes to midnight. This can be understood from photochemistry as summarized in section 1. Below 20 hPa, however, the phase is found short after midnight close to the phase of observed temperature variations (Figure 5). This is a strong indication that vertical advection is the dominating process behind the ozone variations at this level because it is below the peak height. Both models are in good agreement with each other and reproduce all features found in the observations. However, the local maximum in amplitude is found at higher levels at around 3 hPa and the amplitudes are substantially smaller than observed below 4 hPa. The phases as derived from the observations and models agree well above 20 hPa and major discrepancies between observations and models are found below this level. But we note that ozone and temperature modeled by MSDOL are in phase which confirms that vertical transport may be the dominating process in the lower stratosphere.

4. Seasonal Investigations

[34] In order to characterize the daily variations in ozone and water vapor for different seasons, data of months 3, 6 and 9 have been averaged over 2–3 years. The coverage of each data set is given in Table 1. In order to sufficiently

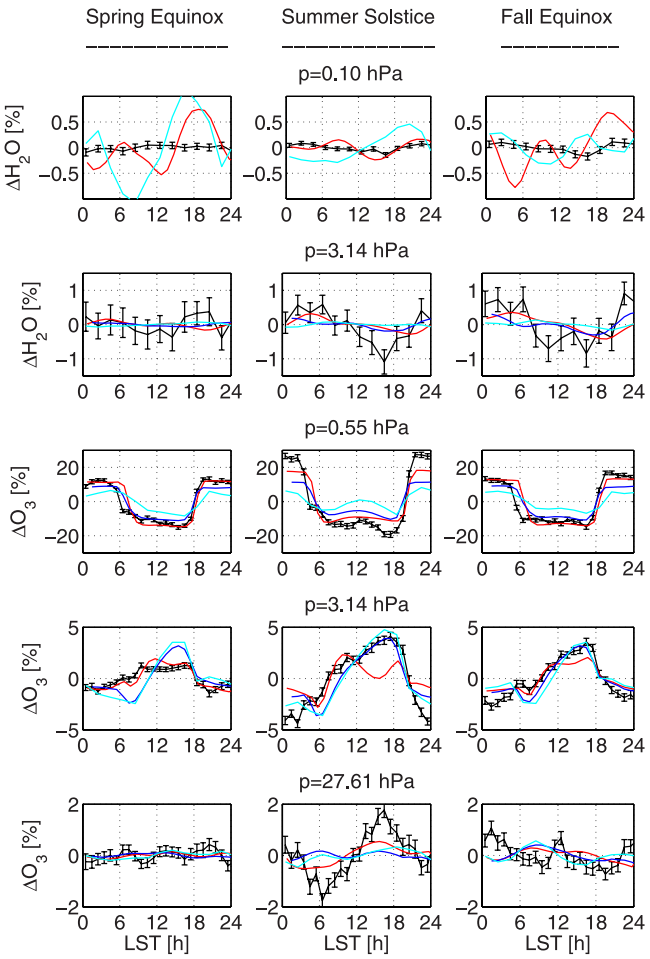

Figure 6. Relative daily variations in water vapor and ozone at constant pressure levels as function of local solar time derived from observations (black line), MSDOL (red line), LMDz (blue line), and SOCOL (cyan line). Data have been averaged over several years (see Table 1) and over months (left) 3, (middle) 6, and (right) 9. The error bars represent the errors of the mean values as described in section 2.3.

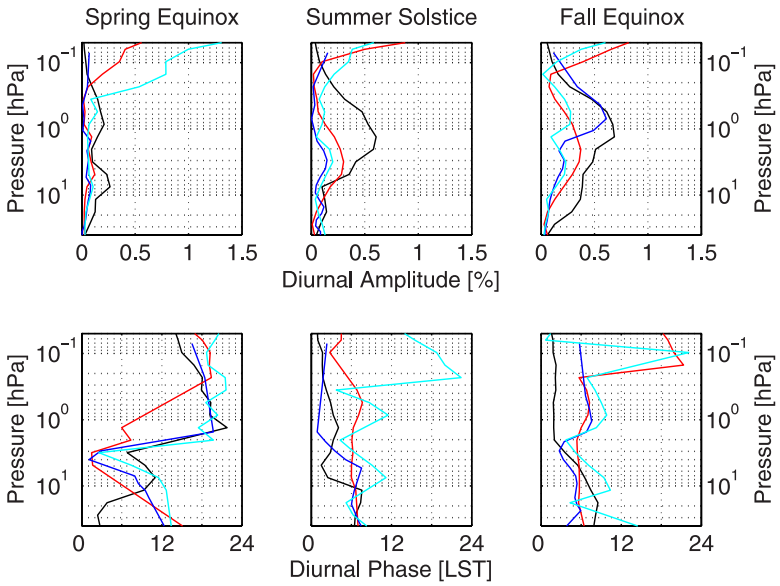

Figure 7. Vertical profiles of the amplitude and phase of the diurnal component of water vapor derived from observations (black line), MSDOL (red line), LMDz (blue line), and SOCOL (cyan line). The plots represent data averaged over several years (see Table 1) and over months (left) 3, (middle) 6, and (right) 9.

reduce noise MIAWARA data have been averaged over the months 3/4, 6/7 and 9/10.

4.1. Time Series

4.1.1. Water Vapor

[35] In case of dynamically driven changes it has to be noted that the seasonality is a superposition of the seasonality in the winds and the gradients of composition. Therefore equinox conditions had to be split in spring and fall equinox as the gradient in water vapor is of different peculiarity for these seasons. The meridional gradient in water vapor, as derived from Aura/MLS data [*Froidevaux et al.*, 2006], is maximal for the months 9 and 10 at 2 hPa reaching 6×10^{-4} ppm/km, twice as large as in spring.

[36] Observations and models reveal no significant cycles during spring equinox (Figure 6). During summer and fall a diurnal component with a minimum at around 18 h is dominating in the observations and the MSDOL and LMDz models. Analysis of the MSDOL data reveals that during the months 6 and 9 the meridional gradients are large and lead to amplitudes of more than 0.3% while in spring amplitudes of the full model do not exceed 0.1% and both meridional and vertical advection are important (not shown here). Only weak cycles are generally observed at 0.10 hPa and maximum amplitudes of 0.1% are found for fall equinox (Figure 6). In contrast to the observations the MSDOL and SOCOL models show amplitudes up to 1% at this level. Again, observed amplitudes are likely to be underestimated because of the lower sensitivity at this level.

4.1.2. Ozone

[37] At 27.61 hPa, no systematic cycle can be found in ozone during spring neither in observational nor in model data. However in summer a clear minimum is found at 6 h followed by a maximum at 16 h which is also simulated by MSDOL with somewhat lower amplitude. Observations reveal a maximum of 1% at 2 h during fall equinox when the models are in good agreement with each other showing similar amplitudes as observed but are 6 h behind the observations. At 3.14 hPa the enhancement during daytime is largest in summer when the solar zenith angle is smallest and hence the production of odd oxygen is largest. This is clearly reproduced by LMDz and SOCOL while MSDOL shows strong daytime depletion during all seasons. The smallest amplitude is observed during spring equinox, where again a flat-shaped daytime enhancement could be an indication of catalytic destruction of ozone. However, there is no evidence for daytime ozone depletion in LMDz and SOCOL data.

4.2. Vertical Structure

[38] The vertical profiles of the diurnal amplitude and phase derived from daily variations in ozone and water vapor are shown in Figures 7 and 8 (see also section 3.2).

4.2.1. Water Vapor

[39] The largest amplitudes in water vapor are observed during summer and fall at 1–2 hPa. The double-peak structure observed during C1 (Figure 5) is not characteristic for fall equinox but we note that the amplitude at 10 hPa is clearly largest during this season. MSDOL shows a very similar behavior but the local maximum is predicted somewhat lower at 2–3 hPa. Below 1 hPa SOCOL and LMDz show the small amplitudes during all periods which is a consequence of the small meridional gradients in the H_2O field of SOCOL and LMDz (see Figure 9). The strong increase above 0.2 hPa found in MSDOL and SOCOL data is expected to be present in the real atmosphere as well because of the strong vertical gradient in H_2O and the amplification of the tidal winds with increasing altitude. However, the measurement fails to detect this increase because its sensitivity gradually decreases above 0.10 hPa.

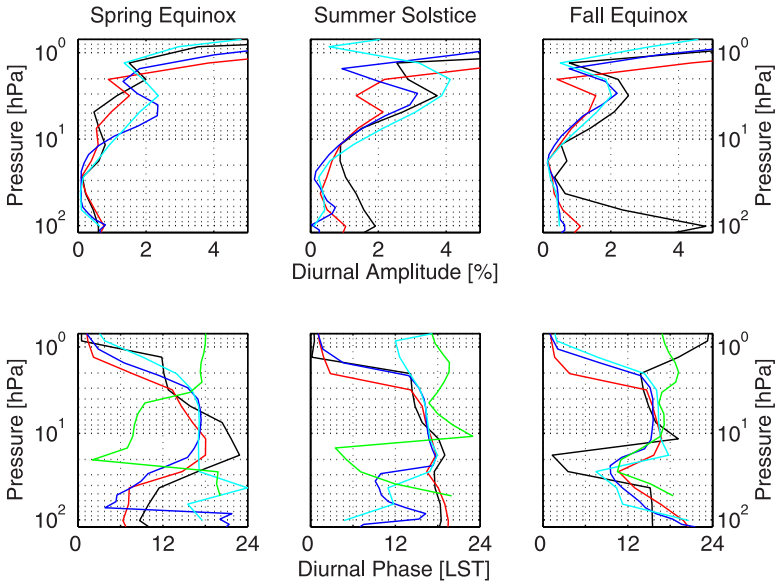

Figure 8. Same as Figure 7 but for ozone. The temperature phases derived from SABER temperature data (green line) are also shown.

LMDz is not reliable at the upper levels because it is close to its upper boundary at 0.10 hPa.

4.2.2. Ozone

[40] Observations and models reveal generally a consistent picture of daily ozone variations in the middle atmosphere. Large amplitudes of 10 to 20% are found above 2 hPa where ozone is dramatically depleted during daytime. Daytime maxima occur below 2 hPa and are largest in summer but do not exceed 4% in amplitude. Large discrepancy in amplitude is found among all data sets during spring equinox between 3 and 6 hPa and between observations and models below 20 hPa in summer and fall. The phases are very consistent above 20 hPa and disagree substantially below 20 hPa in spring.

[41] The diurnal phase of temperature derived from SABER data is shown as well in Figure 8. Observations reveal the following phase relationship between ozone and temperature: The phase lag of 12 h in spring at 6 hPa shrinks to 6 h at 40 hPa where ozone leads temperature. The phase profiles in summer reveal no systematics. During fall equinox temperature and ozone are out of phase at 20 hPa and change to in phase at 40 hPa. MSDOL and SOCOL behave very similar in terms of the phase relationship between O_3 and *T*. However, in MSDOL the phase lag does not exceed 6 h indicating that photochemical equilibrium is never maintained (see section 1). SOCOL indicates a strong temperature dependence of ozone below 20 hPa in summer where ozone leads temperature by 6 h.

4.3. Comparison With GSWM

[42] The seasonal evolution of amplitude and phase in H_2O at 65 km has been investigated and compared to the GSWM (Figure 10). For this purpose observed daily variations have been decomposed in a diurnal and a semidiurnal

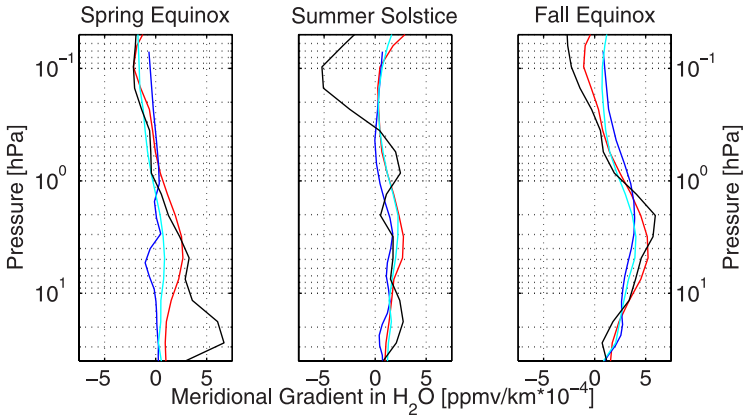

Figure 9. Vertical profiles of the meridional gradient derived from MSDOL (red line), LMDz (blue line), SOCOL (cyan line), and Aura/MLS measurements (black line) for months 3 (spring equinox), 6 (summer solstice), and 9 (fall equinox).

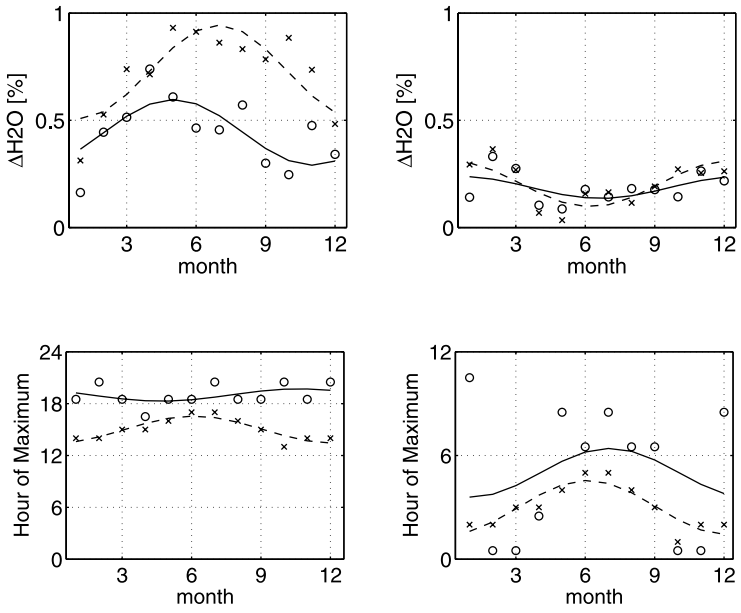

Figure 10. Monthly mean (left) diurnal and (right) semidiurnal (top) amplitudes and (bottom) phases at 65 km derived from MIAWARA (circles) and from GWSM winds and H_2O volume mixing ratio gradients (Aura/MLS data) according to equation (2) (crosses). For comparison, harmonic functions with periods of 12 months are fitted to the observational data (solid line) and to the model data (dashed line).

component. For comparison amplitudes and phases of wind-induced composition changes have been estimated according to equation (2) using winds from GSWM and the vertical gradient in volume mixing ratio derived from radiometer data. For comparison a harmonic function with a 12 month period has been fitted to the amplitudes and phases. The results derived on altitude surfaces differ from those derived on pressure surfaces because the pressure surface itself is moving up and down as part of the tidal wave. As a consequence the amplitudes derived on pressure surfaces are generally smaller than those derived on altitude surfaces as shown in Figure 10.

[43] Enhanced diurnal amplitudes are observed during summer while semidiurnal amplitudes are maximal in winter (Figure 10). Diurnal phases are very constant throughout the whole year and semidiurnal phases show a strong seasonality. The agreement with GSWM is generally good. Maximal diurnal amplitudes are predicted somewhat later in the year and are generally larger by 50%. Good agreement is found for the semidiurnal amplitude in terms of amplitude and seasonality. A constant offset between observations and GSWM is found for the phases but the seasonal dependence is in good agreement.

5. Summary and Conclusions

[44] The correct treatment of tides in atmospheric general circulation models is necessary for an improved description of interactions between radiative, chemical and dynamical processes on timescales from hours to days. Also, a correct parameterization of processes operating on short timescales in the atmosphere are in turn important for the simulation of long-term changes. In this study, data from ground based radiometers and lidar have been analyzed in order to characterize daily variations in middle atmospheric water vapor, ozone and temperature over the Alps and detailed comparisons with the chemistry-climate models MSDOL, LMDz and SOCOL have been made.

[45] Water vapor is a long-lived trace gas in the stratosphere. Consequently, changes on a timescale of a day are governed by advection. By means of a simplified advection scheme and on the basis of MSDOL winds and water vapor fields, we have found that the daily variations of H_2O are mainly induced by meridional advection in the stratosphere and by vertical advection in the mesosphere. We have also noted that both LMDz and MSDOL underestimate absolute values of water vapor over the whole vertical range by $\approx$20% compared to observations while SOCOL overestimates water vapor by more than 10% compared to the observations. This reflects the difficulty to properly model middle atmospheric water vapor.

[46] Photochemistry is the dominant process for daily variations in ozone in the middle-upper stratosphere and mesosphere. Two regimes can be identified: Above 2 hPa, ozone is dramatically depleted during daytime while, below 2 hPa, a daytime enhancement in ozone is observed. This behavior is attributed to the $[O]/[O_3]$ ratio which depends strongly on air density and UV levels; the ratio increases with height. The transition layer below which dynamical and temperature-dependent processes become more important than photochemistry lies at $\approx$10 hPa and varies with season (being located at lower levels in summer).

[47] One of the main focuses of this work was to analyze the first CAWSES campaign of September/October 2005. In the stratosphere, at 3.14 hPa, the daily variations of water vapor show amplitudes between 0.5 and 1% with a distinct minimum at around 18 h. The observed vertical structure of the diurnal amplitude showed an enhancement in the stratosphere and a decrease toward the mesopause. This behavior is likely to be due to the interaction of daily oscillations in the meridional wind and the meridional

gradient in water vapor. All models under consideration could qualitatively simulate these features. However, in terms of absolute magnitude, significant differences were found between the observations and the model simulations and between the different model simulations. In the mesosphere the observed variations are generally smaller than what is predicted by the models even under consideration of the low sensitivity of the measurement in the mesosphere.

[48] The main feature in O_3 daily variations, at 3.14 hPa, is an enhancement during the day reaching a maximum of about 2% shortly before 18 h. All models were able to reproduce these features and also to resolve some small-scale features. However, there are still uncertainties pertaining to the contributions of the different catalytic cycles of ozone destruction.

[49] We also performed an analysis on seasonal timescales. The results indicate that uncertainties exist with respect to the amplitude of daily variations in stratospheric water vapor which arise partly from the differences in the meridional gradient that in turn is mainly governed by the large-scale meridional circulation. In case of the H_2O observations, an underestimation of the amplitudes in the lower mesosphere arises from the influence of a priori information to the retrieval.

[50] Generally, in the case of ozone, the seasonal dependencies of the diurnal variations derived from the observations and in the model simulations are found to be rather consistent. Diurnal variations in the stratosphere can be as large as 4% in summer and large variability is noted in terms of catalytic destruction during daytime depending on season and model. The absolute values of water vapor, the source of HO_x, could not explain the differences. Large discrepancies are also found in the day-night differences of mesospheric ozone and in the amplitude and phase in the lower stratosphere where dynamical and temperature-dependent processes play an important role.

[51] Monthly mean diurnal and semidiurnal amplitudes and phases in water vapor at 65 km were derived at different seasons. The diurnal amplitudes are found to be maximal in summer, which is consistent with the GSWM simulations. However, the maximum occurs 2 months later compared to the observations. Model-calculated diurnal amplitudes are twice as large as observed; this is probably related to the limited sensitivity of the measurement at this altitude. Diurnal phases do not exhibit a distinct seasonal cycle in contrast to the semidiurnal phase that changes by 4 h throughout the whole year. There is a systematic offset in diurnal and semidiurnal phase of 2 to 4 h between GSWM simulations and MIAWARA observations.

[52] **Acknowledgments.** This work has been supported by the Swiss National Science foundation under grant 200020-115882/1 as well as through the project SHOMING financed by MeteoSwiss within GAW. We acknowledge the support of the European Commission through the GEOMON Integrated Project under the 6th Framework Program (contract FOP6-2005-Global-4-036677). The development and maintenance of the CCM SOCOL is supported by ETH Zurich grant PP-1/04-1. We would like to thank J.M. Forbes for providing SABER data and M.A. Hagan for providing GSWM data.

References

Barnett, J. J., and J. A. Pyle (1975), The temperature dependence of the ozone concentration near the stratopause, *Q. J. R. Meteorol. Soc.*, *101*, 245–257.

Bertaux, J. L., A. Hauchecorne, A. Mangin, C. Cot, O. Talagrand, P. Simon, E. Kyrölä, H. Roscoe, O. Hembise, and B. P. Brasseur (1999), The MSDOL project: Assimilation of GOMOS ozone data in a 3-D chemistry-transport model, *Phys. Chem. Earth*, *24*, 435–437.

Buehler, S. A., P. Eriksson, T. Kuhn, A. von Engeln, and C. Verdes (2005), ARTS, the atmospheric radiative transfer simulator, *J. Quant. Spectrosc. Radiat. Transfer*, *91*, 65–93.

Calisesi, Y. (2003), The stratospheric ozone monitoring radiometer SOMORA: NDSC application document, *Tech. Rep. 2003-11*, Inst. of Appl. Phys., Univ. of Bern, Bern.

Connor, B. J., D. E. Siskind, J. J. Tsou, A. Parrish, and E. E. Rempsberg (1994), Ground-based microwave observations of ozone in the upper stratosphere and mesosphere, *J. Geophys. Res.*, *99*, 16,757–16,770.

Deuber, B., N. Kämpfer, and D. G. Feist (2004), A new 22-GHz radiometer for middle atmospheric water vapour profile measurements, *IEEE Trans. Geosci. Remote Sens.*, *42*, 974–984.

Douglass, A. R., R. B. Rood, and R. S. Stolarski (1985), Interpretation of ozone temperature correlations: 2. Analysis of SBUV ozone data, *J. Geophys. Res.*, *90*, 10,693–10,708.

Egorova, T., E. Rozanov, V. Zubov, and I. Karol (2003), Model for investigating ozone trends (MEZON), *Phys. Atmos. Ocean*, *39*, 323–339.

Egorova, T., E. Rozanov, V. Zubov, E. Manzini, W. Schmutz, and T. Peter (2005), Chemistry-Climate Model SOCOL: A validation of the present-day climatology, *Atmos. Chem. Phys.*, *5*, 1557–1576.

Ehhalt, D. H., E. P. Röth, and U. Schmidt (1983), On the temporal variance of stratospheric trace gas concentrations, *J. Atmos. Chem.*, *1*, 27–51.

Eriksson, P., C. Jiménez, and S. A. Buehler (2005), Qpack, a general tool for instrument simulation and retrieval work, *J. Quant. Spectrosc. Radiat. Transfer*, *91*, 47–64.

Eyring, V., et al. (2006), Assessment of temperature, trace species, and ozone in chemistry-climate model simulations of the recent past, *J. Geophys. Res.*, *111*, D22308, doi:10.1029/2006JD007327.

Fels, S. B., and M. D. Schwarzkopf (1981), An efficient, accurate algorithm for calculating CO_2 15 μm band cooling rates, *J. Geophys. Res.*, *86*, 1205–1232.

Froidevaux, L., M. Allen, S. Berman, and A. Daughton (1989), The mean ozone profile and its temperature sensitivity in the upper stratosphere and lower mesosphere: An analysis of lims observations, *J. Geophys. Res.*, *94*, 6389–6417.

Froidevaux, L., et al. (2006), Early validation analyses of atmospheric profiles from EOS MLS on the aura satellite, *IEEE Trans. Geosci. Remote Sens.*, *44*, 1106–1121.

Gille, S. T., A. Hauchecorne, and M.-L. Chanin (1991), Semidiurnal and diurnal tidal effects in the middle atmosphere as seen by Rayleigh lidar, *J. Geophys. Res.*, *96*, 7579–7587.

Groves, G. V. (1982), Hough components of water vapor heating, *J. Atmos. Terr. Phys.*, *44*, 281–290.

Groves, G. V. (1995), A global reference atmosphere from 18 to 80 km, *Tech. Rep. TR-85-0129*, Air Force Geophys. Lab., Bedford, Mass.

Groves, G. V. (1997), Final scientific report, *Tech. Rep. 84-0045*, Air Force Off. of Sci. Res., Bolling Air Force Base, Washington, D. C.

Hagan, M. E., M. D. Burrage, J. M. Forbes, J. Hachney, W. J. Randel, and X. Jhang (1999), GSWM-98: Results for migrating solar tides, *J. Geophys. Res.*, *104*, 6813–6828.

Hauchecorne, A., and M.-L. Chanin (1980), Density and temperature profiles obtained by lidar between 35 and 70 km, *Geophys. Res. Lett.*, *7*, 565–568.

Hecht, J. H., et al. (1998), A comparison of atmospheric tides inferred from observations at the mesopause during ALOHA-93 with the model predictions of the TIME-GCM, *J. Geophys. Res.*, *103*, 6307–6321.

Hedin, A. E. (1991), Extension of the MSIS thermosphere model into the middle and lower atmosphere, *J. Geophys. Res.*, *96*, 1159–1172.

Hedin, A. E. (1996), Empirical wind model for the upper, middle, and lower atmosphere, *J. Atmos Terr. Phys.*, *58*, 1421–1447.

Hines, C. O. (1997), Doppler spread parameterization of gravity wave momentum deposition in the middle atmosphere. Part 1: Basic formulation, *J. Atmos Terr. Phys.*, *59*, 371–386.

Hocke, K., N. Kämpfer, D. G. Feist, Y. Calisesi, J. H. Jiang, and S. Chabrillat (2006), Temporal variance of lower mesospheric ozone over Switzerland during winter 2000/2001, *Geophys. Res. Lett.*, *33*, L09801, doi:10.1029/2005GL025496.

Hocke, K., et al. (2007), Comparison and synergy of stratospheric ozone measurements by satellite limb sounders and the ground-based microwave radiometer SOMORA, *Atmos. Chem. Phys.*, *7*, 4117–4131.

Hourdin, F., and A. Armengaud (1999), The use of finite-volume methods for atmospheric advection trace species: 1. Tests of various formulations in a general circulation model, *Mon. Weather Rev.*, *127*, 822–837.

Huang, F. T., C. A. Reber, and J. Austin (1997), Ozone diurnal variations observed by UARS and their model simulation, *J. Geophys. Res.*, *102*, 12,971–12,985.

Huang, F. T., H. G. Mayr, J. M. Russel III, M. G. Mlynczak, and C. A. Reber (2008), Ozone diurnal variations and mean profiles in the mesosphere, lower thermosphere, and stratosphere, based on measurements from SABER on TIMED, *J. Geophys. Res.*, *113*, A04307, doi:10.1029/2007JA012739.

Keckhut, P., et al. (1996), Semi-diurnal and diurnal temperature tides (30–55 km): Climatology and effect on uars-lidar data comparisons, *J. Geophys. Res.*, *101*, 10,299–10,310.

Lefèvre, F., G. P. Brasseur, I. Folkins, A. K. Smith, and P. Simon (1994), Chemistry of the 1991/1992 stratospheric winter: Three-dimensional model simulations, *J. Geophys. Res.*, *99*, 8183–8195.

Lefèvre, F., F. Figarol, K. S. Carslaw, and T. Peter (1998), The 1997 Arctic ozone depletion quantified from three-dimensional model simulations, *Geophys. Res. Lett.*, *25*, 2425–2428.

Lott, F. (1999), Alleviation of stationary biases in a GCM through a mountain drag parameterization and a simple representation of mountain lift forces, *Mon. Weather Rev.*, *127*, 788–801.

Lott, F., and M. Miller (1997), A new subgrid scale orographic drag parameterization: Its testing in the ECMWF model, *Q. J. R. Meteorol. Soc.*, *123*, 101–127.

Lott, F., L. Fairhead, F. Hourdin, and P. Levan (2005), The stratospheric version of LMDz: Dynamical climatologies, arctic oscillation, and impact on the surface climate, *Clim. Dyn.*, *25*, 851–868.

Manzini, E., and N. A. McFarlane (1998), The effect of varying the source spectrum of a gravity wave parameterization in a middle atmosphere general circulation model, *J. Geophys. Res.*, *103*, 31,523–31,539.

Marsh, D., A. Smith, and E. Noble (2003), Mesospheric ozone response to changes in water vapor, *J. Geophys. Res.*, *108*(D3), 4109, doi:10.1029/2002JD002705.

McLandress, C. (1997), Seasonal variability of the diurnal tide: Results from the Canadian middle atmosphere general circulation model, *J. Geophys. Res.*, *102*, 29,747–29,764.

Morcrette, J.-J. (1989), Description of the radiative scheme in the ECMWF model, *Tech. Rep. N260165*, 26 pp., Eur. Cent. for Medium-Range Weather Forecasts, Reading, U. K.

Morel, B., H. Bencherif, P. Keckhut, S. Baldy, and A. Hauchecorne (2002), Evidence of tidal perturbations in the middle atmosphere over southern tropics as observed by Rayleigh lidar, *J. Atmos. Sol. Terr. Phys.*, *64*, 1979–1988.

Morel, B., P. Keckhut, H. Bencherif, A. Hauchecorne, G. Megie, and S. Baldy (2004), Investigation of the tidal variations in a 3-Df dynamics-chemistry-transport model of the middle atmosphere, *J. Atmos. Sol. Terr. Phys.*, *66*, 251–265.

Pallister, R. C., and A. F. Tuck (1983), The diurnal variation of ozone in the upper stratosphere as a test of photochemical theory, *Q. J. R. Meteorol. Soc.*, *109*, 271–284.

Prather, M. J. (1981), Ozone in the upper stratosphere and mesosphere, *J. Geophys. Res.*, *86*, 5325–5338.

Randel, W. J. (1990), Kelvin wave-induced trace constituent oscillations in the equatorial stratosphere, *J. Geophys. Res.*, *95*, 18,641–18,652.

Randel, W. J., J. M. Russel, A. Roche, and J. W. Waters (1998), Seasonal cycles and QBO variations in stratospheric CH_4 and H_2O observed in UARS HALOE data, *J. Atmos. Sci.*, *55*, 163–185.

Ricaud, P., G. Brasseur, J. Brillet, J. de La Noë, J.-P. Parisot, and M. Pirre (1994), Theoretical validation of ground-based microwave ozone observations, *Ann. Geophys.*, *12*, 664–673.

Rodgers, C. D. (1976), Retrieval of atmospheric temperature and composition from remote measurements of thermal radiation, *Rev. Geophys.*, *14*, 609–624.

Rood, R. B., and A. R. Douglass (1985), Interpretation of ozone temperature correlations: 1. Theory, *J. Geophys. Res.*, *90*, 5733–5743.

Rozanov, E., V. Zubov, E. M. Schlesinger, F. Yang, and N. Andronova (1999), The UIUC 3-D Stratospheric Chemical Transport Model: Description and evaluation of the simulated source gases and ozone, *J. Geophys. Res.*, *104*, 11,755–11,781.

Rozanov, E., M. Schraner, C. Schnadt, T. Egorova, M. Wild, A. Ohmura, V. Zubov, W. Schmutz, and T. Peter (2005), Assessment of the ozone and temperature variability during 1979–1993 with the chemistry-climate model SOCOL, *Adv. Space. Res.*, *35*, 1375–1384.

Sander, S. P., et al. (2000), Chemical kinetics and photochemical data for use in stratospheric data, supplemented to evaluation 12: Update of key reactions, *JPL Publ., 00-3*, 73 pp.

Schneider, N., F. Selsis, J. Urban, O. Lezeaux, J. de la Noë, and P. Ricaud (1999), Seasonal and diurnal ozone variations: Observations and modeling, *J. Atmos. Chem.*, *50*, 25–47.

Schraner, M., et al. (2008), Chemistry-climate model SOCOL: Version 2.0 with improved transport and chemistry/microphysics schemes, *Atmos. Chem. Phys. Discuss.*, *8*, 11,103–11,147.

Schwarzkopf, M. D., and S. B. Fels (1985), Improvements to the algorithm for computing CO_2 transmissivities and cooling rates, *J. Geophys. Res.*, *90*, 10,541–10,550.

Strobel, D. F. (1978), Parameterization of the atmospheric heating rate from 15 to 120 km due to O_2 and O_3 absorption of solar radiation, *J. Geophys. Res.*, *83*, 6225–6230.

Tiedke, M. (1989), A comprehensive mass flux scheme for cumulus parameterization in large scale models, *Mon. Weather Rev.*, *117*, 1779–1800.

van Leer, B. (1977), Towards the ultimate conservative difference scheme: IV. A new approach to numerical convection, *J. Comput. Phys.*, *23*, 276–299.

Vaughan, G. (1984), Mesospheric ozone—Theory and observation, *Q. J. R. Meteorol. Soc.*, *110*, 239–260.

Zhang, X., J. M. Forbes, M. E. Hagen, J. M. Russel III, S. E. Palo, C. J. Mertens, and M. G. Mlynczak (2006), Monthly tidal temperatures 20–120 km from TIMED/SABER, *J. Geophys. Res.*, *111*, A10S08, doi:10.1029/2005JA011504.

Zhu, X. (1994), An accurate and efficient radiation algorithm for middle atmosphere models, *J. Atmos. Sci.*, *51*, 3593–3614.

Zubov, V. A., E. V. Rozanov, and M. E. Schlesinger (1999), Hybrid scheme for three-dimensional advective transport, *Mon. Weather Rev.*, *127*, 1335–1346.

S. Bekki and M. Marchand, Service d'Aéronomie, University Pierre et Marie Curie, 4, Place Jussieu, F-75252 Paris, France.

T. Egorova, Physical-Meteorological Observatory, World Radiation Center, Dorfstrasse 33, CH-7260 Davos, Switzerland. (t.egorova@pmodwrc.ch)

A. Haefele, K. Hocke, and N. Kämpfer, Department of Microwave Physics, Institute of Applied Physics, University of Bern, Sidlerstrasse 5, CH-3012 Bern, Switzerland. (alexander.haefele@mw.iap.unibe.ch)

P. Keckhut, Service d'Aéronomie, University of Versailles, Saint Quentin, B.P. 3, F-91371 Verrières-le Buisson, France.

B. Morel, Université de la Réunion, 15 avenue René Cassin, BP 7151, F-97715 La Réunion, France. (beatrice.morel@univ-reunion.fr)

E. Rozanov, Institute for Atmospheric and Climate Science, ETH Zurich, CH-8092 Zürich, Switzerland. (e.rozanov@pmodwrc.ch)